An Efficient Multi-Vector-Based Model Predictive Current Control for PMSM Drive

Jun SUN, Yong YANG, Rong CHEN, Xinan ZHANG, Chee Shen LIM, and Jose RODRIGUEZ

***Abstract*—To address the problems of high current harmonics, large torque ripples, and heavy computational burden in the finite control set model predictive control (FCS-MPC), this paper proposes an efficient multi-vector model predictive current control (MPCC) scheme for permanent magnet synchronous motor (PMSM) drive. Firstly, a simple pre-selection method based on the trace of the stator current increment is proposed to obtain the candidate optimal voltage vectors. This pre-selection method avoids the heavy computational burden of evaluating all voltage vectors and is easy to implement. Then, to further reduce the torque ripples and current harmonics, the dwelling time of each voltage vector is achieved in inverse proportion to its cost function. Compared to the standard means, the proposed scheme is able to obtain great performance while greatly decreasing the computational burden and complexity. And its effectiveness is experimentally validated through comparative assessments.**

***Index Terms*—Finite control set model predictive control (FCS-MPC), low complexity, multi-vector control, pre-selection, permanent magnet synchronous motor (PMSM).**

I. Introduction

PERMANENT magnet synchronous motor (PMSM) has been widely applied in electric vehicles and robot industries due to its high torque-to-inertia ratio, structural compactness, and high power density [1], [2]. Especially for high-power traction system, the application of PMSM drives can obtain the benefits of energy saving, comfort, and safety [2]. However, with the increasing requirements on the performance of PMSM drives, traditional control schemes like field-oriented control (FOC) and direct torque control (DTC) have shown limitations in addressing new challenges [3], [4]. Therefore, researches into new technologies of electric drives have been making significant strides recently [5].

Among various control schemes, model predictive control (MPC) schemes have been paid significant attention because of the superiority of simple structure, strong capacity of rejecting disturbance, and fast dynamic response [6], [7]. In general, MPC schemes can be briefly categorized as continuous control set MPC (CCS-MPC) and finite control set MPC (FCS-MPC) [8]. The FCS-MPC, in contrast to CCS-MPC, utilizes online enumeration to identify the optimal voltage vector which handles the certain control problem defined through the cost function [9], [10]. Earlier FCS-MPC variants usually do not consider pulse width modulation (PWM), leading to simpler microprocessor-based implementation, and a fast dynamic response similar to most direct control schemes, such as DTC [11].

For the traditional FCS-MPC, the utilization of only one voltage vector in the entire control cycle brings about large torque ripples and high harmonics [13]. Over the past years, a substantial number of improvement works have been reported to overcome these problems. A common way is to raise the quantity of the available voltage vectors based on the 8 basic voltage vectors [12]–[18]. For instance, the scheme of synthesizing virtual voltage vectors is introduced in [12] to expand the quantity of available voltage vectors. These virtual voltage vectors are contained into the control set that will be evaluated to minimize the cost function. [13] extends the quantity of virtual voltage vectors to 38. And due to the more voltage vectors are available, the selected optimal voltage vector can better fit the reference value. Furthermore, [14] applies the virtual voltage vectors scheme on the basis of 32 basic voltage vectors, which can obtain better system performance in a five-phase two-level inverter. Nevertheless, the above ways typically lead to an increased computational burden to the real-time control system [15].

Hence, several works have attempted to achieve a tradeoff between system performance and computing efforts when increasing the quantity of virtual voltage vectors [16]–[18]. In [16], the enumeration times is reduced from 37 to 13 through an optimal selection strategy while well maintaining the steady-state and transient system performance. In [17] and [18], the region of the optimal voltage vector can be identified through introducing the deadbeat control principle, which decreases the quantity of candidate voltage vectors. Unfortunately, there is still some problems such as imperfect matching of the optimal

Manuscript received June 26, 2023; revised August 15, 2023; accepted September 12, 2023. Date of publication March 30, 2024; date of current version September 29, 2023. This work was supported in part by the National Natural Science Foundation of China under Grant 52377195, Grant 51977136, and Grant 52007127, in part by XJTLU RDF-21-02-018, in part by through projects FB0008, 1210208 and 1221293. *(Corresponding authors: Yong Yang and Rong Chen.)*

J. Sun, Y. Yang, and R. Chen are with the School of Rail Transportation, Soochow University, Suzhou 215131, China (e-mail: jsun98@stu.suda.edu.cn; yangy1981@suda.edu.cn; chrong@suda.edu.cn).

X. Zhang is with the Department of Electrical, Electronic and Computer Engineering, University of Western Australia, Perth, WA 6009, Australia (e-mail: xinan.zhang@uwa.edu.au).

C. S. Lim is with School of Electrical and Electronic Engineering, Xi'an Jiaotong-Liverpool University, Suzhou 215123, China (e-mail: cheeshen.lim@xjtlu.edu.cn).

J. Rodriguez is with Faculty of Engineering, Universidad San Sebastian Santiago, Santiago 8370146, Chile (e-mail: jose.rodriguezp@uss.cl).

Digital Object Identifier 10.24295/CPSSTPEA.2023.00044

voltage vector and complicated calculation process [18].

Another effective solution to address the shortcomings of conventional FCS-MPC is through using multiple voltage vectors to synthesize optimal output voltage vector within each control period. [19]–[23] integrate the duty cycle mechanism into FCS-MPC to extend the magnitude of the output voltage vector. In [19], the optimal voltage vector and dwelling time are determined by considering the projection relationship of the stator current error vector, resulting improved performance. Based on the conventional predictive torque control (PTC), [22] introduces the deadbeat principle to calculate the dwelling time, thus reducing the torque ripples. However, the application of deadbeat principle is usually sensitive to the system parameters, thereby resulting in poor robustness. Furthermore, the phase of the synthesized voltage vector in the above schemes is restricted due to the exclusive use of zero voltage vector [24].

Therefore, the combination of the two active voltage vectors is added into the selection strategy in [25]–[28] to further extend the synthesized range of the optimal voltage vector. In [24], the number of traversals is reduced to 25 by considering the similarity of voltage vector combinations while maintaining low torque ripples. [27] applies a pre-defined look-up table to reconstruct the three-phase duty cycle based on the deadbeat principle, and achieves a fixed switching frequency.

In addition, some studies consider the combination of three voltage vectors to further reduce the steady-state error. In [29], a three-vector scheme is proposed around the power error to completely eliminate the steady-state error. However, the calculation of dwelling time is very tedious. [30] obtains the candidate optimal voltage vector by using the deadbeat principle and cost function, respectively, to improve the performance and suppress the zero-sequence current (ZSC). In [31], the virtual voltage vectors are constructed to expand the selection of candidate voltage vector sequence. Meanwhile, through a hierarchical optimization, the accuracy of the optimal output voltage vector is improved. Furthermore, [32] and [33] complete pre-selection based on the stator flux error to reduce the computational burden, but the calculation of dwelling time is not easy.

In this paper, an efficient model predictive current control (MPCC) scheme based on multi-vector is proposed to overcome the shortcomings of the afore-mentioned aspects. The major contributions are listed as follows:

a) The proposed scheme employs an effective pre-selection method to determine the candidate voltage vectors. Through tracking the increment of the stator current, the approach avoids the evaluation process of redundant voltage vectors. Hence, compared with the existing schemes, the proposed scheme has lower computational burden and complexity.

b) The dwelling time for each candidate voltage vector in the proposed scheme is obtained on the basis of the cost function, which not only reduces the algorithm complexity, but also enhances the parameter robustness. Moreover, the proposed scheme can achieve a fixed switching frequency through rearranging the switching sequence.

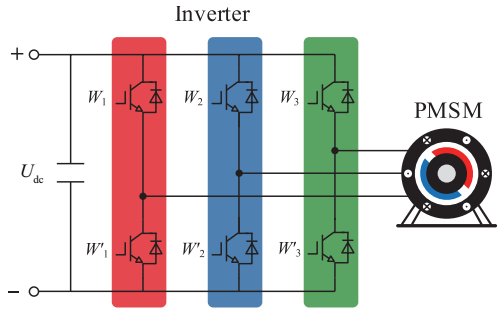

Fig. 1. Three-phase two-level PMSM drives.

c) The effectiveness of the proposed scheme is verified through the experimental comparison with the existing MPCC schemes.

The remaining parts of this paper are organized as follows: The mathematical model of inverter and PMSM are described in Section II. After that, the principles of single-voltage-vector and multi-voltage-vector MPCC (MVV-MPCC) are introduced in Section III. In Section IV, an efficient multi-vector MPCC scheme is proposed. Then, the comparative experimental results of different schemes are presented to verify the proposed scheme in Section V. Finally, conclusions are drawn in Section VI.

II. Mathematical Models of Inverter and PMSM

The topology of three-phase two-level PMSM drives is shown in Fig. 1, and the basic output voltage vectors of the inverter can be defined as

$$\begin{cases} V_i = \dfrac{2}{3} U_{\mathrm{dc}} \left(W_1 + W_2 a + W_3 a^2\right) \\ a = e^{i2\pi/3} \end{cases} \tag{1}$$

where $V_i (i = 0,...,7)$ represents the output voltage vector; U_{dc} represents the dc bus voltage; $W_i (i = 1,2,3)$ represents the switching state of the inverter.

A surface-mounted PMSM (SPMSM) is applied in this paper. Under the premise of ignoring the hysteresis losses and rotor eddy current. The dynamic mathematical model of SPMSM in the *d*-*q* reference frame can be described as

$$\begin{cases} \dfrac{\mathrm{d}i_d}{\mathrm{d}t} = \left(u_d - R_{\mathrm{s}} i_d + \omega_{\mathrm{e}} L_{\mathrm{s}} i_q\right) / L_{\mathrm{s}} \\ \dfrac{\mathrm{d}i_q}{\mathrm{d}t} = \left(u_q - R_{\mathrm{s}} i_q - \omega_{\mathrm{e}} L_{\mathrm{s}} i_d - \omega_{\mathrm{e}} \psi_{\mathrm{f}}\right) / L_{\mathrm{s}} \\ T_{\mathrm{e}} = \dfrac{3}{2} p \psi_{\mathrm{r}} i_q \end{cases} \tag{2}$$

where u_d,u_q represent the stator *d*- and *q*-axis voltages; i_d,i_q represent the stator *d*- and *q*-axis currents; L_{s} represent the stator inductances; ω_{e} represents the electrical angular velocity; ψ_{f} represents the rotor flux; R_{s} represents the stator winding resistance; T_{e} represents the electromagnetic torque; p is the number of pole pairs.

When the sampling period is set short enough in a discrete system, the electrical angular velocity ω_e can be considered constant during each sampling period. Then, the discretization of the PMSM' s current prediction formula can be obtained by adopting the forward Euler scheme in the *d-q* reference frame, approximately, which can be derived as

$$i^{k+1} = C_1 i_s^k + C_2 u_s^k + C_3 \tag{3}$$

where

$$i_s^{k+1} = \begin{bmatrix} i_d^{k+1} & i_q^{k+1} \end{bmatrix}^T$$

$$u_s^k = \begin{bmatrix} u_d^k & u_q^k \end{bmatrix}^T,\ i_s^k = \begin{bmatrix} i_d^k & i_q^k \end{bmatrix}^T$$

and

$$C_1 = \begin{bmatrix} 1 - R_s T_s / L_s & \omega_e T_s \\ -\omega_e T_s & 1 - R_s T_s / L_s \end{bmatrix}$$

$$C_2 = \begin{bmatrix} T_s / L_s & 0 \\ 0 & T_s / L_s \end{bmatrix},\ C_3 = \begin{bmatrix} 0 \\ -\omega_e \psi_f T_s / L_s \end{bmatrix}$$

where i_d^k, i_q^k are the stator *d*- and *q*-axis currents at discrete time instant *k*; u_d^k, u_q^k are the stator *d*- and *q*-axis voltages at time instant *k*; i_d^{k+1}, i_q^{k+1} are the predicted stator *d*- and *q*-axis currents at time instant *k*+1; T_s is the sampling period.

III. Single and Double Voltage Vector Based MPCC

A. Single-Voltage-Vector MPCC Scheme

The conventional MPCC scheme utilizes the MPC controller to regulate the current and the PI controller to regulate the speed. For the single-voltage-vector model predictive current control (SVV-MPCC), it selects the single voltage vector from the basic control set as the optimal voltage vector. The control set contains two zero voltage vectors and six non-zero voltage vectors. Among them, it can be considered that the two zero voltage vectors are equivalent in function. SVV-MPCC substitutes the voltage vectors of the control set into (3) to obtain the predicted values of *d*- and *q*-axis currents. Meanwhile, the error between the reference current and the predicted current is evaluated by the cost function designed to meet control demand. In real-time applications, the one cycle digital delay needs to be compensated through the prediction of one more step. Then, the cost function can be described as

$$J = \left\| i_d^{\text{ref}} - i_d^{k+2} \right\|^2 + \left\| i_q^{\text{ref}} - i_q^{k+2} \right\|^2 \tag{4}$$

where i_d^{ref}, i_q^{ref} represent the reference stator *d*- and *q*-axis currents.

After enumeration optimization, the single voltage vector that minimizes the cost function will act as the optimal voltage vector in the next control period.

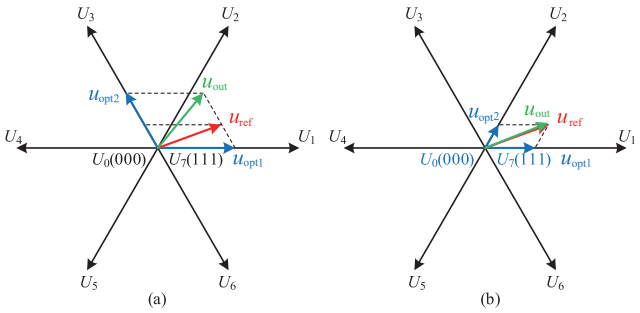

Fig. 2. Schematic diagram of multi voltage vectors synthesis. (a) DVV-MPCC and (b) TVV-MPCC.

B. Conventional MVV-MPCC Scheme

In a single control period, the SVV-MPCC can only apply one basic voltage vector, leading to degraded torque and current responses. As shown in Fig. 2, compared with the SVV-MPCC, the application of MVV-MPCC can reduce the difference between the output voltage vector and reference voltage vector, consequently enhancing the system performance. According to the number of voltage vectors involved in the synthesis, the MVV-MPCC can be divided into double-voltage-vector MPCC (DVV-MPCC) and three-voltage-vector MPCC (TVV-MPCC).

Compared with the conventional DVV-MPCC [24], [25], the TVV-MPCC [31] employs the deadbeat principle to precisely calculate the dwelling time of basic voltage vectors, which are used to synthesize the desired output voltage vector, as shown in Fig. 2.

To implement the TVV-MPCC, the first step involves deducing the slope of the stator *d-q* axis current corresponding to the action of the zero voltage vector. It leads to

$$\begin{cases} S_{d_0} = \left. \dfrac{\mathrm{d}i_d}{\mathrm{d}t} \right|_{u_d = 0} = (\omega_e L_s i_q - R_s i_d)/L_s \\ S_{q_0} = \left. \dfrac{\mathrm{d}i_q}{\mathrm{d}t} \right|_{u_q = 0} = (-R_s i_q - \omega_e L_s i_d - \omega_e \psi_f)/L_s \end{cases} \tag{5}$$

where S_{d0}, S_{q0} denotes the slope of stator *d-q* axis current under zero vector action.

Similarly, the slope of the stator *d-q* axis current under the action of the active voltage vector can also be obtained as

$$S_{di,qi} = \left. \frac{\mathrm{d}i_{d,q}}{\mathrm{d}t} \right|_{u_{d,q} = u_{di,q}} = S_{d0,q0} + \frac{u_{di,qi}}{L_s} \tag{6}$$

where $S_{di,\,qi,\,i=1,\ldots,6}$ represents the slope of stator *d-q* axis current under the active voltage vector.

After that, on the basis of the deadbeat principle and considering one cycle delay, we have $i_s^{k+2} = i_s^{\text{ref}}$. So, the current increment in each control cycle can be described as

$$\begin{cases} \Delta i_d = i_d^{\text{ref}} - i_d^{k+1} = S_{dj} t_j + S_{dk} t_k + S_{d0} t_0 \\ \Delta i_q = i_q^{\text{ref}} - i_q^{k+1} = S_{qj} t_j + S_{qk} t_k + S_{q0} t_0 \\ T_s = t_j + t_k + t_0 \end{cases} \tag{7}$$

where $S_{dj,\,qj}$, $S_{dk,\,qk}$ are the slopes of the two adjacent voltage vectors in a sector; t_j, t_k are the dwelling time of the two adjacent voltage vectors; t_0 is the dwelling time of the zero voltage vector.

Then, the dwelling time of each voltage vector is obtained, respectively, as

$$\begin{cases} t_j = \dfrac{1}{\gamma}\Big[\Delta i_d(S_{qk}-S_{q0})+\Delta i_q(S_{d0}-S_{dk})+ \\ \qquad T_s(S_{q0}S_{dk}-S_{qk}S_{d0})\Big] \\ t_k = \dfrac{1}{\gamma}\Big[\Delta i_d(S_{q0}-S_{qj})+\Delta i_q(S_{dk}-S_{d0})+ \\ \qquad T_s(S_{qj}S_{d0}-S_{q0}S_{dj})\Big] \\ \gamma = S_{q0}S_{dk}+S_{qj}S_{d0}+S_{qk}S_{dj}- \\ \qquad S_{qj}S_{dk}-S_{qk}S_{d0}-S_{q0}S_{dj} \end{cases} \tag{8}$$

It should be noted that the current increment calculated by the deadbeat principle may exceed the regulation threshold. Therefore, the total dwelling time of the active voltage vectors needs to be limited within [0, T_s].

Hence, the synthesized voltage vector can be expressed as

$$u_{syn} = \frac{1}{T_s}(u_j t_j + u_k t_k + u_{0/7} t_0) \tag{9}$$

where u_j, u_k represent the adjacent stator voltage vector within each sector in the *d*-*q* frame.

After substituting (9) into (3), the optimal voltage vectors can be obtained through minimizing (4).

Therefore, as shown in Fig. 2, compared with the DVV-MPCC, the TVV-MPCC exhibits the capability to adjust the phase and amplitude of the synthesized voltage vector simultaneously by inserting the zero voltage vector. This benefit is also reflected in the ability of tracking the reference current. As shown in Fig. 3, due to the limitation of the fixed control period, the DVV-MPCC may generate a large error between the predicted current and the reference current. In contrast, the TVV-MPCC can adjust the action time of each voltage vector more flexibly to minimize this error. However, despite the conventional TVV-MPCC can effectively improve the control performance, it still suffers from having heavy computation burden.

IV. Proposed Control Scheme

In this section, an efficient MVV-MPCC scheme is designed to overcome the drawbacks of the schemes discussed in Section III. The proposed strategy identifies the candidate voltage vectors based on a fast pre-selection method, and utilizes the cost function to calculate the dwelling time of each voltage vector, which results in a low computational burden, great control performance and robustness.

A. Control Algorithm of Proposed Scheme

As analyzed in Section III, the schemes using multiple voltage vectors synthesis have proven effective in reducing the torque ripples and current harmonics compared with SVV-MPCC. Moreover, compared to the DVV-MPCC, the conventional TVV-MPCC can further expand the range of modulation by flexibly adjusting the dwelling time of the candidate voltage vectors, leading to better performance.

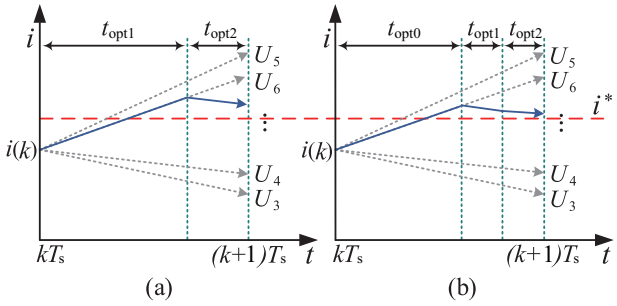

Fig. 3. Schematic diagrams of the comparison of stator current error. (a) DVV-MPCC and (b) the proposed scheme.

However, the generation of the optimal voltage vector sequence in the TVV-MPCC still needs iterative evaluation, which introduces a large computational burden. Furthermore, the computation of dwelling time for each voltage vector is reliant on the slope of the stator current. As shown in (5), (6), (8), the calculation process is very tedious and exhibits high parameter sensitivity.

Different from the conventional TVV-MPCC, in the proposed scheme, the candidate voltage vectors are obtained by a simple pre-selection method firstly. Specifically, in the stationary reference frame, there are

$$u_s = R_s i_s + \frac{\mathrm{d}\psi_s}{\mathrm{d}t} \tag{10}$$

$$\psi_s = L_s i_s + \psi_r e^{i\theta_e} \tag{11}$$

where ψ_s is the stator flux.

The discrete model of (10) is

$$\Delta\psi_s = u_s T_s + R_s i_s T_s \tag{12}$$

Since the sampling time is usually very small in the real control system, it can be assumed that the change of stator flux is linearly related to the stator voltage vector. Meanwhile, assuming that the rotor rotation angle is neglected in a single control cycle, and using the speed loop output as the reference stator current, then according to (11) we can obtain

$$\Delta\psi_s = L_s(i_s^* - i_s^{k+1}) \tag{13}$$

According to (12) and (13), it can be considered that there is an approximately linear relationship between the increment of stator current and the reference stator voltage vector.

$$\Delta i_s = i_s^* - i_s^{k+1} \approx u_s^{\mathrm{ref}} \frac{T_s}{L_s} \tag{14}$$

In (14), ignoring the effect of scalar coefficients, it can be assumed that the same phase information exists between the

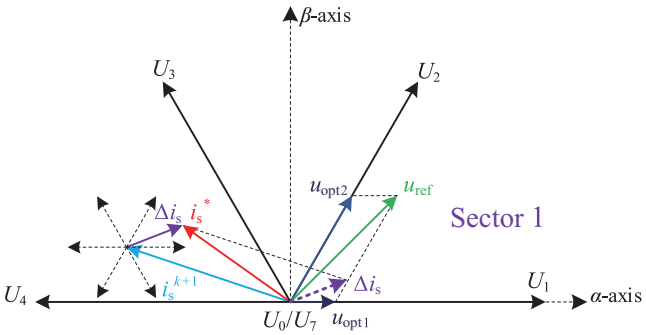

Fig. 4. Schematic diagram of the proposed pre-selection method.

TABLE I
SECTOR AND OPTIMAL VOLTAGE VECTORS

Sector	Judgment conditions	Optimal voltage vectors
1	$\Delta i_{s\beta} \geqslant 0, \Delta i_{s\alpha} \leqslant \sqrt{3}\Delta i_{s\beta}$	$\boldsymbol{U}_1$, $\boldsymbol{U}_2$, $\boldsymbol{U}_{0/7}$
2	$\Delta i_{s\beta} \geqslant 0, \Delta i_{s\alpha} > \sqrt{3}\Delta i_{s\beta}, \Delta i_{s\alpha} > -\sqrt{3}\Delta i_{s\beta}$	$\boldsymbol{U}_2$, $\boldsymbol{U}_3$, $\boldsymbol{U}_{0/7}$
3	$\Delta i_{s\beta} \geqslant 0, \Delta i_{s\alpha} \leqslant -\sqrt{3}\Delta i_{s\beta}$	$\boldsymbol{U}_3$, $\boldsymbol{U}_4$, $\boldsymbol{U}_{0/7}$
4	$\Delta i_{s\beta} < 0, \Delta i_{s\alpha} \geqslant \sqrt{3}\Delta i_{s\beta}$	$\boldsymbol{U}_4$, $\boldsymbol{U}_5$, $\boldsymbol{U}_{0/7}$
5	$\Delta i_{s\beta} < 0, \Delta i_{s\alpha} < \sqrt{3}\Delta i_{s\beta}, \Delta i_{s\alpha} < -\sqrt{3}\Delta i_{s\beta}$	$\boldsymbol{U}_5$, $\boldsymbol{U}_6$, $\boldsymbol{U}_{0/7}$
6	$\Delta i_{s\beta} < 0, \Delta i_{s\alpha} \geqslant -\sqrt{3}\Delta i_{s\beta}$	$\boldsymbol{U}_6$, $\boldsymbol{U}_1$, $\boldsymbol{U}_{0/7}$

increment of the stator current and the reference stator voltage vector. Therefore, the increment of the stator current can be used to confirm the position of the reference stator voltage vector, thus completing the pre-selection of the candidate optimal voltage vectors.

A simple look-up table can be used to confirm the spatial distribution of the reference stator voltage vector. Assuming that the active voltage vectors divide the vector space into six uniform sectors, the sector in which the increment of stator current is located can be uniquely identified by the projection on the $\alpha\beta$-axis. Furthermore, according to the basic principle of vector synthesis, any voltage vector inside this sector can be obtained by combined two boundary active voltage vectors and a zero voltage vector. Hence, the proposed scheme defines the zero voltage vector and two boundary active voltage vectors in the sector where the increment of stator current is located as the candidate optimal voltage vectors. As shown in Fig. 4, assuming that the calculated increment of stator current is in sector 1, then the U_1, U_2, $U_{0/7}$ are selected as candidate voltage vectors. A more detailed correspondence is presented in Table I.

The dwelling time of each candidate voltage vector is adjusted through the value of cost function in the proposed scheme to reduce the torque ripples and current harmonics. According to (4), the cost function of each candidate voltage vector can be obtained as

$$j_i = \left\| i_d^{\text{ref}} - i_d^{k+2} \right\|^2 + \left\| i_q^{\text{ref}} - i_q^{k+2} \right\|^2, i = 0,1,2 \tag{15}$$

The deviation of the reference current from the predicted current is indirectly reflected through the cost function under the action of the voltage vector. In fact, the voltage vector component with a large cost function should occupy a smaller proportion for maximizing the tracking ability of the predicted current to the reference current, which can be described as an inversely proportional relationship

$$\begin{cases} \gamma_0 = (1/j_0)/(1/j_0 + 1/j_1 + 1/j_2) \\ \gamma_1 = (1/j_1)/(1/j_0 + 1/j_1 + 1/j_2) \\ \gamma_2 = (1/j_2)/(1/j_0 + 1/j_1 + 1/j_2) \end{cases} \tag{16}$$

where γ_i (i = 0,1,2) are the proportions of dwelling time of the three voltage vector components; j_i (i = 0,1,2) are the cost function value of the three voltage vector components.

B. Pulse Generation With Fixed Switching Frequency

In conventional MPCC, the switching frequency is variable because of the utilization of only one voltage vector in each control cycle, which results in the increase of current harmonics. For the proposed scheme, the type and quantity of the voltage vectors that are adopted to synthesize the final output voltage vector is fixed in a single control cycle. According to the principle of volt-second balance, the vector switching sequence is output symmetrically to achieve a fixed switching frequency. For example, suppose that the final output voltage vector is situated in sector 1, as shown in Fig. 5(a), since zero vectors have the same effect, the switching sequence of the output voltage vector is 111-110-100-000-100-110-111. Define t_i (i = 0,1,2) represents the dwelling time of each voltage vector component, we have

$$t_i = \gamma_i T_s, \ i = 0, \ 1, \ 2 \tag{17}$$

where t_0 here refers to the dwelling time of the zero voltage vector.

By arranging the output switching sequences in each sector in a similar way as shown in Fig. 5, the constant switching frequency can be guaranteed.

C. Discussion

In general, the proposed scheme multi-vector MPCC scheme is very simple. Firstly, based on the trace of the increment of stator current, the proposed scheme applies a simple pre-selection method to determine the candidate voltage vectors, efficiently reducing the computational burden. Secondly, the cost function is used to calculate the dwelling time for each voltage vector in the proposed scheme, which results in less complexity and parameter sensitivity compared with the deadbeat method. Moreover, the proposed scheme can obtain a fixed switching frequency through rearranging the output switching sequence according to a simple look-up table. Fig. 6 depicts the control block diagram of the whole system, which can be summarized as follows: 1) Measure the three-phase stator current, speed and electrical angle; 2) Add delay compensation; 3) Calculate the increment of stator current; 4) Confirm the sector and obtain the candidate voltage vector; 5)

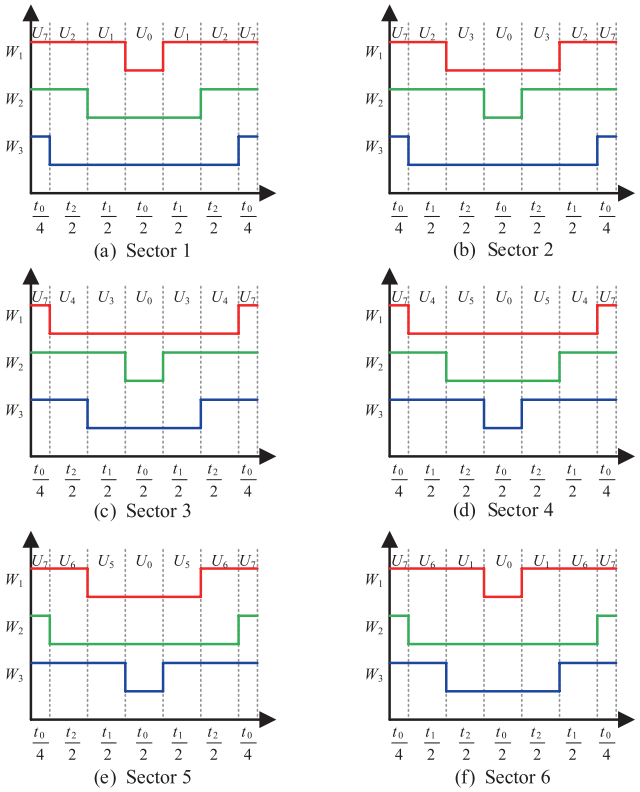

Fig. 5. Schematic diagram of fixed switching frequency sequence.

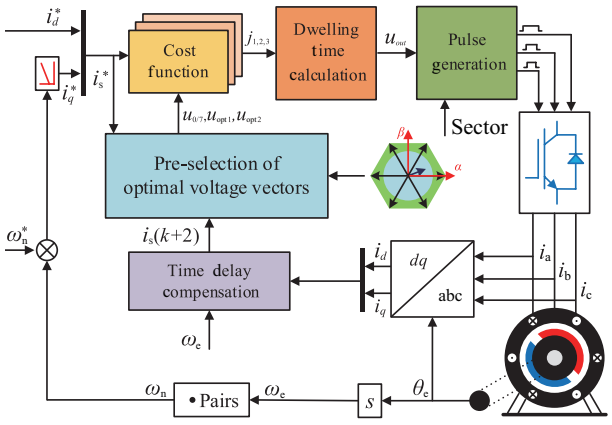

Fig. 6. Control block diagram of the proposed scheme.

Evaluate the cost function and calculate the dwelling time; 6) Rearrange the switching sequence to meet a fixed switching frequency.

V. Experimental Results

This section reveals the experimental results of the proposed scheme that are obtained using the experimental platform shown in Fig. 7. The experimental platform utilizes TI TMS320F28335 as the microcontroller. The PMSM parameters used in the experiment are presented in the Table II. Besides, the sampling frequency is set to 10 kHz. The proposed scheme is compared with SVV-MPCC, DVV-MPCC, a three

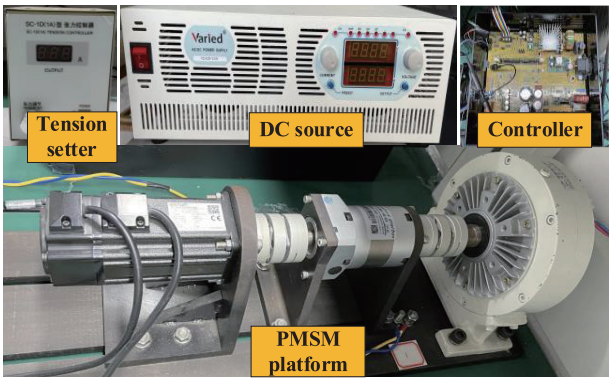

Fig. 7. Experimental platform.

TABLE II
Parameter of the Experimental System

Parameters	Value
DC voltage u_{dc}	320 V
d-axis inductance L_d	6.5 mH
q-axis inductance L_q	6.5 mH
Stator resistance R_s	2.35 Ω
Rotor flux ψ_f	0.07876 Wb
Pole pairs p	4
Inertia coefficient J	0.0003 kg·m^2
Rated speed	3000 r/min
Rated torque	1.27 N·m
Sample time T_s	0.0001 s

TABLE III
Algorithm Execution Time (μs)

Terms	SVV MPCC	DVV MPCC	TVV MPCC[31]	DB MPCC	Proposed scheme
AD sampling	3.10	3.10	3.10	3.10	3.10
Time delay compensation	1.82	1.82	1.82	1.82	1.82
Evaluation of optimal voltage vectors	9.15	24.34	12.56	5.74	6.22
Dwelling time calculation	-	3.86	4.32	2.96	1.71
Total	14.07	33.12	21.80	13.62	12.85

voltage vector scheme (TVV-MPCC[31]), an SVPWM based deadbeat MPCC (DB-MPCC) to highlight the superiority. For all schemes, the PI parameters of the speed regulator are consistent and i_d^{ref} is zero.

A. Execution Time

Table III shows the detailed execution time of SVV-MPCC, DVV-MPCC, TVV-MPCC[31], DB-MPCC and the proposed

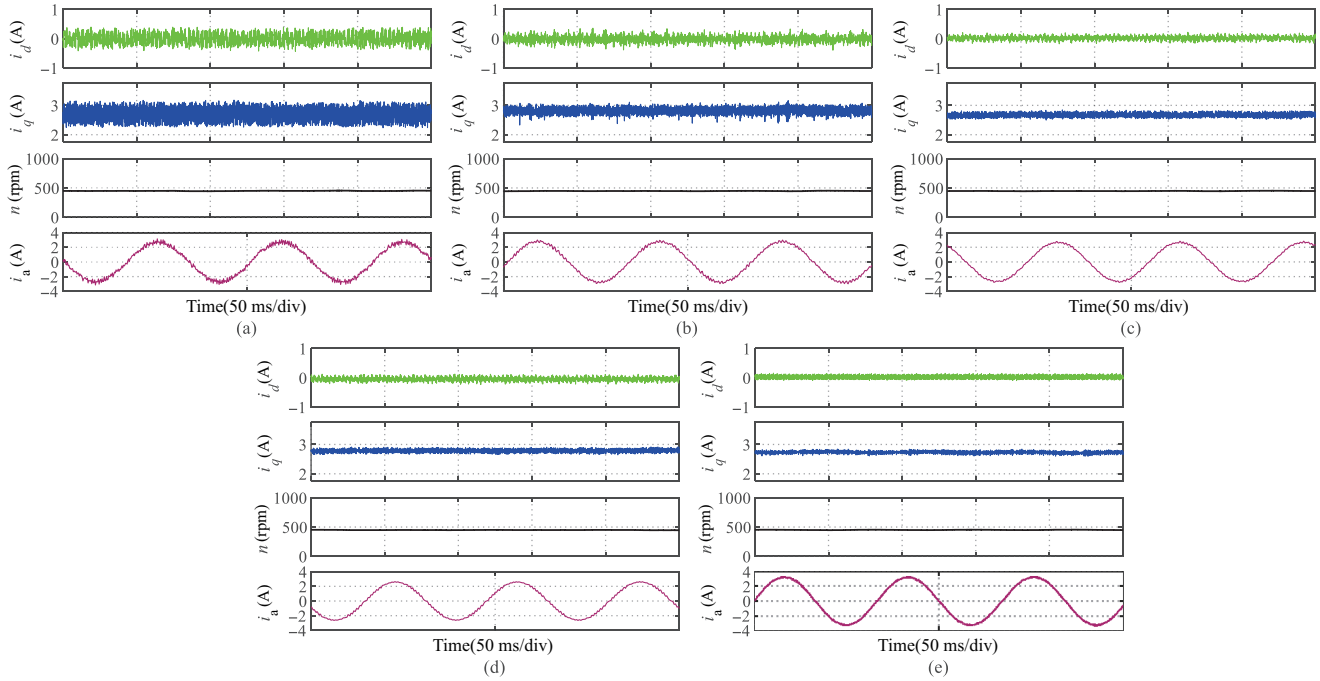

Fig. 8. Comparative waveforms of *d-q* axis currents, phase-A stator current, and speed at 450 rpm. (a) SVV-MPCC. (b) DVV-MPCC. (c) TVV-MPCC[31]. (d) DB-MPCC. (e) The proposed scheme.

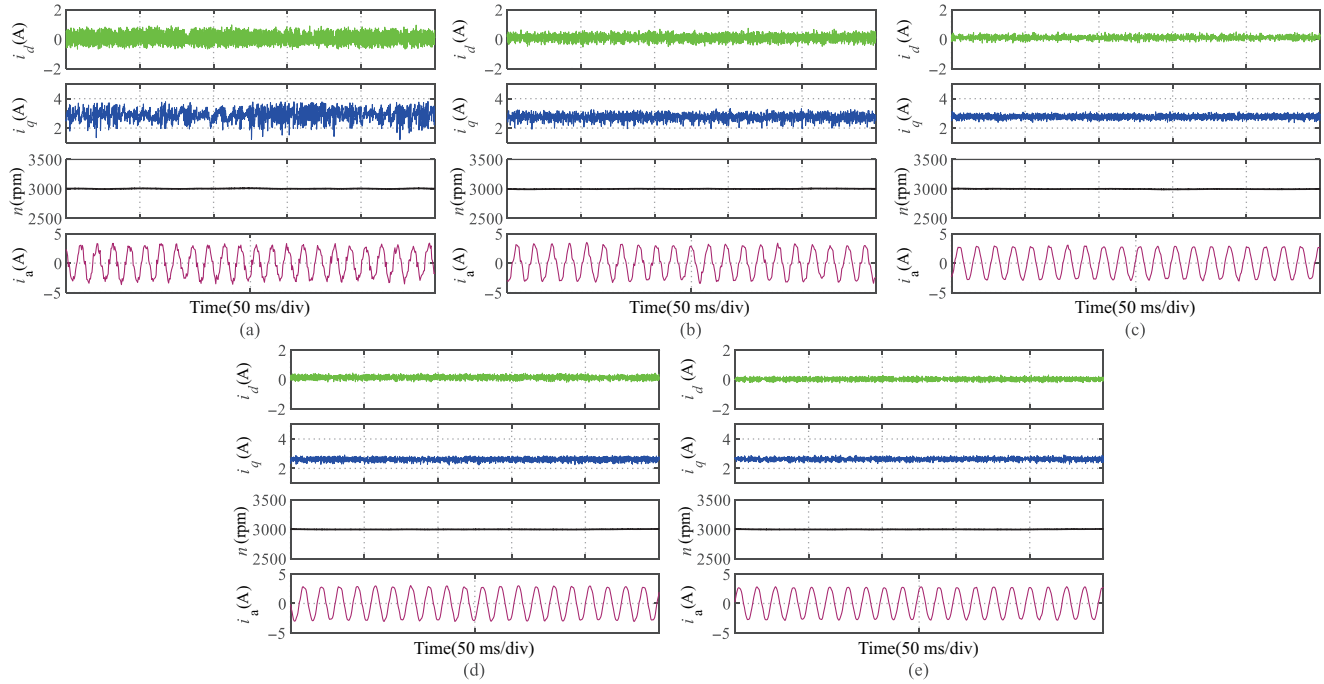

Fig. 9. Comparative waveforms of *d-q* axis currents, phase-A stator current, and speed at 3000 rpm. (a) SVV-MPCC. (b) DVV-MPCC. (c) TVV-MPCC[31]. (d) DB-MPCC. (e) The proposed scheme.

scheme. For accurately evaluating the amount of computation of three schemes, the measured execution time is averaged over multiple tests. The execution time of SVV-MPCC, DVV-MPCC, TVV-MPCC[31], DB-MPCC and the proposed scheme is 14.07, 33.12, 21.8, 13.62 and 12.85 μs, respectively. It is observable that the proposed scheme as a fast algorithm significantly decreases the computational burden of MPCC and is more suitable for real-time applications.

B. Steady-State Performance

The steady-state performances of all schemes under 450 rpm and 3000 rpm with a load of about 1.27 N·m are presented in Figs. 8 and 9, respectively. These figures include the waveforms of speed, phase-A current, and stator *d*- and *q*-axis currents for different schemes. By observing the waveforms, it is evident that the proposed scheme exhibits reduced stator

TABLE IV
THD OF PHASE CURRENT AND STANDARD DEVIATION OF Q-AXIS STATOR CURRENT UNDER DIFFERENT SPEED

Scheme	450 rpm		900 rpm		1500 rpm		2250 rpm		3000 rpm	
	THD(%)	Standard deviation of i_q(A)	THD(%)	Standard deviation of i_q(A)	THD(%)	Standard deviation of i_q(A)	THD(%)	Standard deviation of i_q(A)	THD(%)	Standard deviation of i_q(A)
SVV-MPCC	16.57	0.2657	16.32	0.2625	17.08	0.2844	17.37	0.2867	18.73	0.2943
DVV-MPCC	11.62	0.1542	12.39	0.1577	11.88	0.1673	12.31	0.1764	13.91	0.1766
TVV-MPCC[31]	5.78	0.0634	6.45	0.0635	6.53	0.0622	6.51	0.0647	6.69	0.0732
DB-MPCC	5.63	0.0546	5.72	0.0558	5.67	0.0569	5.82	0.0588	6.13	0.0594
Proposed scheme	5.51	0.0513	5.49	0.0537	5.68	0.0567	5.75	0.0572	5.92	0.0581

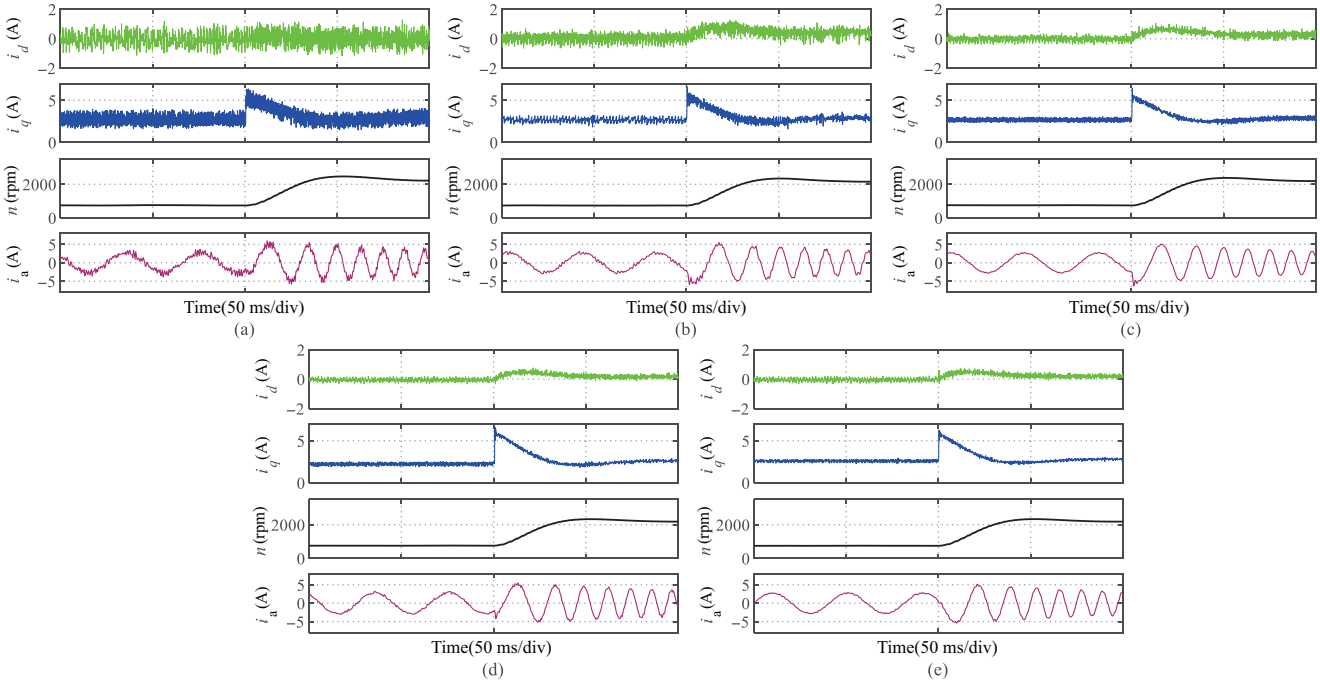

Fig. 10. Comparative waveforms in dynamic state. speed 750 rpm → 2250 rpm. (a) SVV-MPCC. (b) DVV-MPCC. (c) TVV-MPCC[31]. (d) DB-MPCC. (e) The proposed scheme.

d- and *q*-axis current ripples and smoother phase-A current compared to SVV-MPCC, DVV-MPCC for the given speed conditions. Meanwhile, compared with DB-MPCC and TVV-MPCC[31], it can be seen that the proposed scheme produces lower ripples in the stator *d*-*q* axis current.

To further demonstrate the great steady-state performance of the proposed scheme, the fast Fourier transform (FFT) analysis of phase-A current is carried out, and the standard deviation of the stator *q*-axis current is calculated at different speeds. The results are listed in Table IV.

From the Table IV, it can be seen that the standard deviation of the stator *q*-axis current of the proposed scheme is about 0.0554 A on average, which is significantly smaller than its counterparts of SVV-MPCC and DVV-MPCC. Similarly, the proposed scheme also has lower total harmonic distortion (THD) compared to other schemes, which is 5.67% on average. Therefore, it can be proved that the proposed multi-vector MPCC scheme effectively reduces the torque ripples and current harmonics in the steady state.

C. Dynamic Performance

Different dynamic tests are performed to further validate the effectiveness of the proposed scheme. Fig. 10 shows the waveforms of the reference speed stepping from 750 rpm to 2250 rpm. It can be seen that all the schemes have similar dynamic response process. However, compared with other schemes, the proposed scheme is able to maintain lower stator *d*- and *q*-axis current ripples and smoother phase-A current during the process. Fig. 11 shows the response of the reference stator *q*-axis current stepping from 1.5 A to 2.5 A. The dynamic test results show that the proposed scheme can maintain great dynamic response while requiring less computational burden due to the utilization of pre-selection method and dwelling time calculation approach.

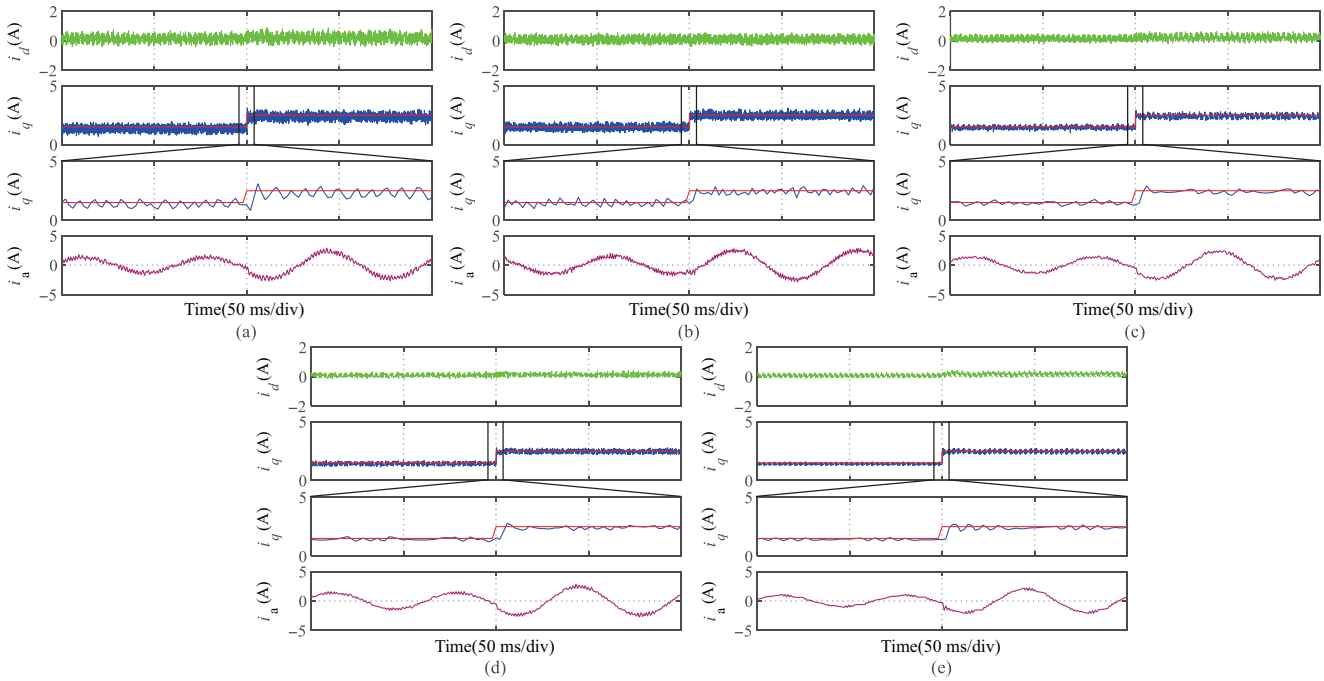

Fig. 11. Comparative waveforms in dynamic state. i_{qref}: 1.5A →2.5A. (a) SVV-MPCC. (b) DVV-MPCC. (c) TVV-MPCC[31]. (d) DB-MPCC. (e) The proposed scheme.

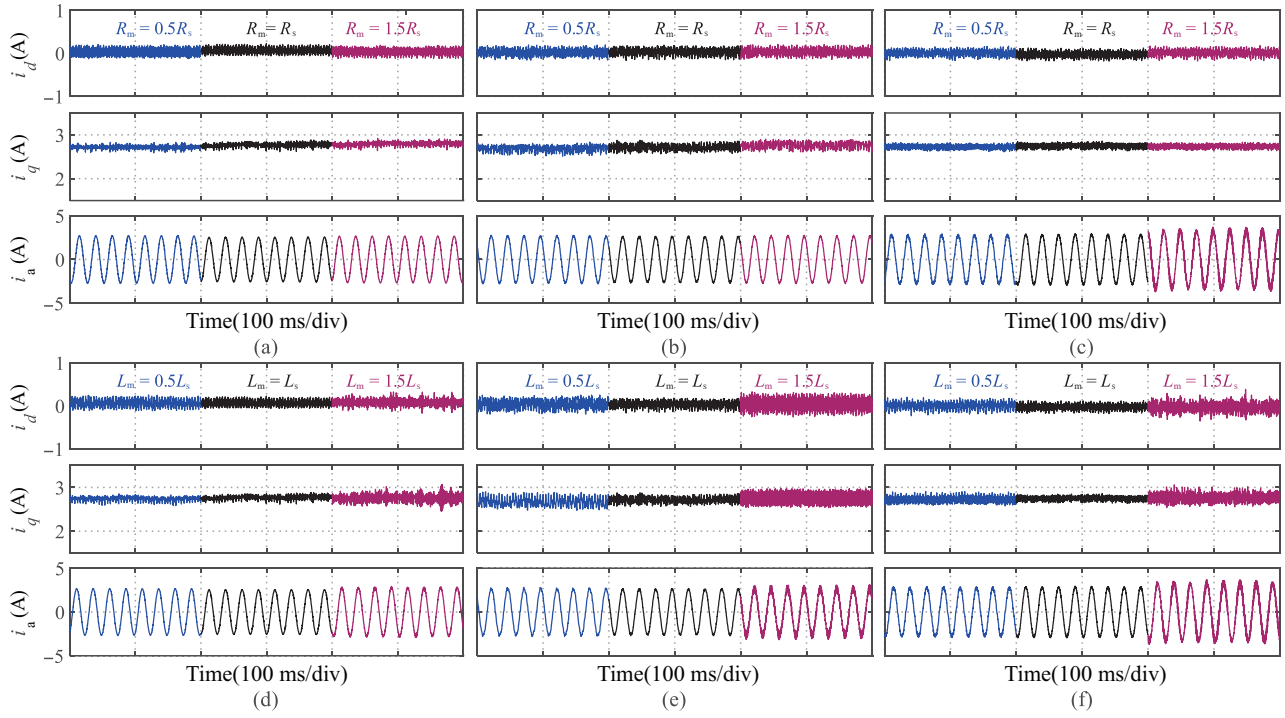

Fig. 12. Comparative waveforms with variable model parameters. (a) the proposed scheme (change R_s). (b) TVV-MPCC[31] (change R_s). (c). DB-MPCC (change R_s). (d) The proposed scheme (change L_s). (e) TVV-MPCC[31] (change L_s). (f) DB-MPCC (change L_s).

D. Parameter Robustness

The experimental results of robustness to model parameter variations are depicted in Fig. 12. Specifically, Fig. 12(a), (b), (c) presents the performance of the proposed scheme, DB-MPCC and TVV-MPCC[31] when the motor stator resistance is 0.5 R_s, R_s, and 1.5 R_s, respectively. As shown in Fig. 12(a), (b), (c), it is observable that the proposed scheme is almost unaffected by the stator resistance change and has lower stator *d-q* axis current ripples and phase-A current harmonics compared with the DB-MPCC, TVV-MPCC[31]. Furthermore, Fig. 12(d), (e), (f) presents the system performance when the motor stator inductances are 0.5L_s, L_s, and 1.5L_s, respectively.

It can be seen that the torque ripples and current harmonics of both DB-MPCC and TVV-MPCC[31] increase significantly when the stator inductance raises. However, the proposed scheme can still maintain great control performance. Therefore, it can be proved that the proposed scheme has good robustness to parameter variations.

VI. CONCLUSIONS

In this paper, an efficient multi-vector MPCC scheme is proposed for PMSM drives. Compared with the conventional multi-vector schemes, the proposed scheme significantly reduces the computational burden through employing a pre-selection method based on the increment of stator current. Meanwhile, the cost function is applied to adjust the dwelling time of the candidate voltage vectors in the proposed scheme, which reduces the complexity and parameter sensitivity of the algorithm. By combining three voltage vectors within a single control period, the proposed scheme decreases the torque ripples and current harmonics. And the experimental results validate the superior performance of the proposed scheme under various operating conditions. Consequently, the proposed scheme effectively improves the steady-state and dynamic performances of FCS-MPCC with less computational burden.

REFERENCE

[1] Z. Zhang, J. Rodríguez, and R. Kennel, "Advanced control strategies for direct-drive PMSG wind turbine systems: Direct predictive torque control approaches," in *CPSS Transactions on Power Electronics and Applications*, vol. 2, no. 3, pp. 217–225, Sept. 2017.

[2] K. -M. Choo and C. -Y. Won, "Design and analysis of electrical braking torque limit trajectory for regenerative braking in electric vehicles with PMSM drive systems," in *IEEE Transactions on Power Electronics*, vol. 35, no. 12, pp. 13308–13321, Dec. 2020.

[3] Z. Wang, J. Chen, M. Cheng, and K. T. Chau,"Field-oriented control and direct torque control for paralleled VSIs fed PMSM drives with variable switching frequencies," in *IEEE Transactions on Power Electronics*, vol. 31, no. 3, pp. 2417–2428, Mar. 2016.

[4] W. Deng, J. Tang, and W. Cheng, "An enhanced rotating vector-based direct torque control for matrix converter-fed PMSM drives using virtual pulsating vectors," in *CPSS Transactions on Power Electronics and Applications*, vol. 8, no. 1, pp. 65–73, Mar. 2023.

[5] P. Karamanakos and T. Geyer, "Guidelines for the design of finite control set model predictive controllers," in *IEEE Transactions on Power Electronics*, vol. 35, no. 7, pp. 7434–7450, Jul. 2020.

[6] S. Vazquez, J. Rodriguez, M. Rivera, L. G. Franquelo, and M. Norambuena, "Model predictive control for power converters and drives: Advances and trends," in *IEEE Transactions on Industrial Electronics*, vol. 64, no. 2, pp. 935–947, Feb. 2017.

[7] W. Luo and M. Zhou, "Multi-vector based model predictive control for nested neutral point piloted converters with constant switching frequency," in *CPSS Transactions on Power Electronics and Applications*, vol. 8, no. 3, pp. 222–233, Sept. 2023.

[8] A. A. Ahmed, B. K. Koh, and Y. I. Lee, "A comparison of finite control set and continuous control set model predictive control schemes for speed control of induction motors," in *IEEE Transactions on Industrial Informatics*, vol. 14, no. 4, pp. 1334–1346, Apr. 2018.

[9] X. Zhang, H. Bai, and M. Cheng, "Improved model predictive current control with series structure for PMSM drives," in *IEEE Transactions on Industrial Electronics*, vol. 69, no. 12, pp. 12437–12446, Dec. 2022.

[10] Q. Teng, H. Yang, and J. Tian, "Nonlinear function integral sliding mode-based model predictive current control for PMSM drives with DC-bus voltage observer," in *CPSS Transactions on Power Electronics and Applications*, vol. 7, no. 4, pp. 399–408, Dec. 2022.

[11] X. Zhang, Y. Cheng, Z. Zhao, and K. Yan, "Optimized model predictive control with dead-time voltage vector for PMSM drives," in *IEEE Transactions on Power Electronics*, vol. 36, no. 3, pp. 3149–3158, Mar. 2021.

[12] D. Casadei, G. Serra, and K. Tani, "Implementation of a direct control algorithm for induction motors based on discrete space vector modulation," in *IEEE Transactions on Power Electronics*, vol. 15, no. 4, pp. 769–777, Jul. 2000.

[13] Z. Zhou, C. Xia, Y. Yan, Z. Wang, and T. Shi, "Torque ripple minimization of predictive torque control for PMSM with extended control set," in *IEEE Transactions on Industrial Electronics*, vol. 64, no. 9, pp. 6930–6939, Sept. 2017.

[14] W. Wang, Y. Fan, S. Chen, and Q. Zhang, "Finite control set model predictive current control of a five-phase PMSM with virtual voltage vectors and adaptive control set," in *CES Transactions on Electrical Machines and Systems*, vol. 2, no. 1, pp. 136–141, Mar. 2018.

[15] Y. Zhang, H. Jiang, and H. Yang, "Model predictive control of PMSM drives based on general discrete space vector modulation," in *IEEE Transactions on Energy Conversion*, vol. 36, no. 2, pp. 1300–1307, Jun. 2021.

[16] I. Osman, D. Xiao, K. S. Alam, S. M. S. I. Shakib, M. P. Akter, and M. F. Rahman, "Discrete space vector modulation-based model predictive torque control with no sub-optimization," in *IEEE Transactions on Industrial Electronics*, vol. 67, no. 10, pp. 8164–8174, Oct. 2020.

[17] Y. Wang, X. Wang, W. Xie, F. Wang, M. Dou, R. M. Kennel, R. D. Lorenz, and D. Gerling, "Deadbeat model-predictive torque control with discrete space-vector modulation for PMSM drives," in *IEEE Transactions on Industrial Electronics*, vol. 64, no. 5, pp. 3537–3547, May 2017.

[18] M. H. Vafaie, B. M. Dehkordi, P. Moallem, and A. Kiyoumarsi, "Improving the steady-state and transient-state performances of PMSM through an advanced deadbeat direct torque and flux control system," in *IEEE Transactions on Power Electronics*, vol. 32, no. 4, pp. 2964–2975, Apr. 2017.

[19] J. Chen, Y. Qin, A. M. Bozorgi, and M. Farasat, "Low complexity dual-vector model predictive current control for surface-mounted permanent magnet synchronous motor drives," in *IEEE Journal of Emerging and Selected Topics in Power Electronics*, vol. 8, no. 3, pp. 2655–2663, Sept. 2020.

[20] F. Yu, X. Liu, Z. Zhu, and J. Mao, "An improved finite-control-set model predictive flux control for asymmetrical six-phase PMSMs with a novel duty-cycle regulation strategy," in *IEEE Transactions on Energy Conversion*, vol. 36, no. 2, pp. 1289–1299, Jun. 2021.

[21] S. Yan, J. Chen, T. Yang, and S. Y. Hui, "Improving the performance of direct power control using duty cycle optimization," in *IEEE Transactions on Power Electronics*, vol. 34, no. 9, pp. 9213–9223, Sept. 2019.

[22] Y. Zhang and H. Yang, "Model predictive torque control of induction motor drives with optimal duty cycle control," in *IEEE Transactions on Power Electronics*, vol. 29, no. 12, pp. 6593–6603, Dec. 2014.

[23] Y. Zhang, W. Xie, Z. Li, and Y. Zhang, "Low-complexity model predictive power control: Double-vector-based approach," in *IEEE Transactions on Industrial Electronics*, vol. 61, no. 11, pp. 5871–5880, Nov. 2014.

[24] Y. Zhang and H. Yang, "Generalized two-vector-based model-predictive torque control of induction motor drives," in *Proceedings of 2014 IEEE Energy Conversion Congress and Exposition (ECCE)*, Pittsburgh, PA, USA, pp. 3570–3577, 2014.

[25] X. Zhang and B. Hou, "Double vectors model predictive torque control without weighting factor based on voltage tracking error," in *IEEE Transactions on Power Electronics*, vol. 33, no. 3, pp. 2368–2380, Mar. 2018.

[26] Y. Zhang, Y. Peng, and H. Yang, "Performance improvement of two-vectors-based model predictive control of PWM rectifier," in *IEEE Transactions on Power Electronics*, vol. 31, no. 8, pp. 6010–6030, Aug. 2016.

[27] Y. Zhang, D. Xu, and L. Huang, "Generalized multiple-vector-based model predictive control for PMSM drives," in *IEEE Transactions on*

Industrial Electronics, vol. 65, no. 12, pp. 9356–9366, Dec. 2018.
[28] Y. Luo and C. Liu, "Multi-vector-based model predictive torque control for a six-phase PMSM motor with fixed switching frequency," in *IEEE Transactions on Energy Conversion*, vol. 34, no. 3, pp. 1369–1379, Sept. 2019.
[29] X. Wang and D. Sun, "Three-vector-based low-complexity model predictive direct power control strategy for doubly fed induction generators," in *IEEE Transactions on Power Electronics*, vol. 32, no. 1, pp. 773–782, Jan. 2017.
[30] D. Xu, W. Zhao, H. Tang, X. Song, and R. Xue, "Three-vector-based model predictive current control with zero-sequence current suppression for open-winding LPMVM drives," in *IEEE Transactions on Vehicular Technology*, vol. 70, no. 1, pp. 225–236, Jan. 2021.
[31] B. Xu, Q. Jiang, W. Ji, and S. Ding, "An improved three-vector-based model predictive current control method for surface-mounted PMSM drives," in *IEEE Transactions on Transportation Electrification*, vol. 8, no. 4, pp. 4418–4430, Dec. 2022.
[32] S. G. Petkar and V. K. Thippiripati, "Effective multi-vector operated predictive current control of PMSM drive with reduced torque and flux ripple," in *IEEE Transactions on Transportation Electrification*, vol. 9, no. 2, pp. 2217–2227, Jun. 2023.
[33] X. Li, Z. Xue, X. Yan, L. Zhang, W. Ma, and W. Hua, "Low-complexity multivector-based model predictive torque control for PMSM with voltage preselection," in *IEEE Transactions on Power Electronics*, vol. 36, no. 10, pp. 11726–11738, Oct. 2021.

Jun Sun received the B.S. degree in engineering from Soochow University, Suzhou, China, in 2021. He is currently pursuing the M.S. degree in engineering at School of Rail Transportation, Soochow University, Suzhou, China.

His research interest includes model predictive control for motor drives.

Yong Yang received the B.S. degree in automation from Xiangtan University, Xiangtan, China, in 2003, the M.S. degree in electrical engineering from Guizhou University, Guiyang, China, in 2006, and the Ph.D. degree in electrical Engineering from Shanghai University, Shanghai, China, in 2010.

He is currently a full Professor with the School of Rail Transportation, Soochow University. From December 2017 to December 2018, he was a Visiting Scholar with Center for High Performance Power Electronics (CHPPE) of the Ohio State University, Columbus, USA. He has coauthored more than 100 journal and conference papers. His current research interests include model predictive control in power electronic converters, distributed energy resource interfacing and high-performance motor drive control.

Rong Chen was born in Jiangsu, China, in 1983. She received the B.S. degree in communication engineering from Soochow University, Suzhou, China, in 2006, the M.S. degree in communication and information system from Soochow University in 2009, and the Ph.D. degree in signal and information processing from Soochow University in 2013.

Currently, she is an Associate Professor working in the School of Rail Transportation, Soochow University. Her research interests include signal processing and synchronous phasor measuring.

Xinan Zhang received the B.E. degree in electrical engineering and automation from Fudan University, China, in 2008. He received the Ph.D. degree from Nanyang Technological University (NTU), Singapore, in 2014. Then, he worked as postdoc researcher in NTU and the University of New South Wales from 2014 to 2017. He worked as a Lecturer in NTU from June 2017 to September 2019.

Since September 2019, he joined the University of Western Australia as a Senior Lecturer. His research interests include electrical machine drives, control and modulation of power electronic converters and design of hybrid energy storage systems.

Chee Shen Lim received the B.Eng. (Hons.) degree in electrical engineering from the University of Malaya, Kuala Lumpur, Malaysia, in 2009, and the joint-university Ph.D. degrees in power electronics and drives from the university of Malaya, Kuala Lumpur, and Liverpool John Moores University, Liverpool, U.K., in 2013.

From 2013 to 2015, he was a Research Scientist with the Experimental Power Grid Centre, Agency for Science, Technology and Research, Singapore. From 2015 to 2021, he was an Assistant/Associate Professor of electrical and electronic engineering with the University of Southampton Malaysia Campus. He is currently an Associate Professor of electrical and electronic engineering with Xi'an Jiaotong-Liverpool University, China. Dr. Lim serves currently as an Associate Editor of the *IET Electric Power Applications*.

Jose Rodriguez received the Engineer degree in electrical engineering from the Universidad Tecnica Federico Santa Maria, in Valparaiso, Chile, in 1977 and the Dr.-Ing. degree in electrical engineering from the University of Erlangen, Erlangen, Germany, in 1985. He has been with the Department of Electronics Engineering, Universidad Tecnica Federico Santa Maria, since 1977, where he was full Professor and President. Since 2015 to 2019, he was the President of Universidad Andres Bello in Santiago, Chile. Since 2022 he is President of Universidad San Sebastian in Santiago, Chile. He has coauthored two books, several book chapters and more than 700 journal and conference papers. His main research interests include multilevel inverters, new converter topologies, control of power converters, and adjustable-speed drives. He has received a number of best paper awards from journals of the IEEE. Dr. Rodriguez is member of the Chilean Academy of Engineering. In 2014 he received the National Award of Applied Sciences and Technology from the government of Chile. In 2015 he received the Eugene Mittelmann Award from the Industrial Electronics Society of the IEEE. In years 2014 to 2021 he has been included in the list of Highly Cited Researchers published by Web of Science.